AFM Tip Position Control in situ for Effective Nano-Manipulation

Shuai Yuan, Zhidong Wang, Ning Xi, Yuechao Wang, Lianqing Liu

Abstract — The spatial uncertainties of atomic force microscope (AFM) tip position hinder the development of the AFM based nano-manipulation. These uncertainties cannot be corrected at nanoscale using the traditional position sensor, which is used in the macro robot localization. As for that problem, we propose that the AFM tip is used as the sensor to detect the landmark in the sample surface via a local-scan based motion. The landmark positions are used to estimate the tip position in the task frame. The local-scan based observation model is built on the foundation of the tip motion model. These model parameters are calibrated using statistical experiments. Simulation and experimental results show that the proposed method can improve the accuracy of the tip position. Then the influence of the tip position accuracy is analyzed by using nano-manipulation results of the experiments. Furtherly, three important factors in AFM tip based nano-manipulation are discussed. The landmark domain as the first factor is analyzed for assurance of the tip accuracy before nano-manipulation. The second one is studying the contact characteristics between the nanoparticle and the substrate by detecting nano-manipulation force. The last one is taking the tip shape into account for effective manipulation through fine tuning the tip offset. Finally, the experimental results illustrate the effectiveness of the proposed method for fabricating the nano-structures and devices.

Index Terms— AFM based Nano-manipulation, AFM Tip Localization, Stochastic Calibration, Kalman Filter.

The manuscript was written on March 20, 2016. The research work is partially supported by the National Natural Science Foundation of China (Project Codes: 61305125, 61522312, 61433017, 91748212), National Post Doctor Foundation (Project Codes: 2013M530955, 2014T70265)), Universities basic Scientific Research Project (LJZ 2017020) and Chinese Academy of Sciences State Foreign Expert Bureau International Partnership Program for Creative Research Teams.

S. Yuan, Y.C. Wang, L.Q. Liu are the researchers of the State Key Laboratory of Robotics in Shenyang Institute of Automation, Chinese Academy of Sciences, Shenyang, Liaoning Province 110016, China. S. Yuan is also an associate professor of the Information & Control Engineering Institute in Shenyang Jianzhu University, Shenyang, Liaoning Province 110168, China, and is with the graduate school of Chinese Academy of Sciences, Beijing 100001,China.(Email: reidyuan @163.com; ycwang@sia.cn, lqliu@sia.cn).

Z.D. Wang is with Department of Advanced Robotics, Chiba Institute of Technology, Chiba, 275-0016, JAPAN. (Email: zhidong.wang@it-chiba.ac.jp).

N. Xi is with Department of Industrial and Manufacturing Systems Engineering, Emerging Technologies Institute, in Faculty of Engineering, University of Hong Kong, Pokfulam Road, HongKong. (Email: xining@hku.hk).

I. Introduction

AFM tip can be used as an end-effector to manufacture the nano-structure for providing a great potential tool of nano-manipulation independently[1,2] or with scanning electron microscope (SEM) assistance[3]. However, it is difficult to guarantee the tip position accuracy in the allowed range due to the PZT (PbZrTiO3) scanner nonlinearity and system thermal drift, which hinders the development of the AFM based nano-manipulation[4-5]. Based on these problems, the PZT models and thermal drift compensation are proposed to enhance nano-manipulation efficiency.

Because nonlinearity of the PZT driver leads to the tip spatial uncertainties[6], the sensor based closed-loop control and model based compensation methods are developed to reduce the hysteretic and creep effects of the PZT. The closed-loop control method is designed to get highly reliable and robust compensation by mounting a positioning sensor on the scanner. And the tip position relative to the scanner centre axes can only be improved by this method. However, the tip position error in the substrate surface cannot be compensated due to the thermal drift. Also this method can be costly and lead to higher system noise which results in deterioration of the image quality, and even the oscillations in small scan areas[7]. Thus, a method of model based compensation [8, 9] is proposed to compensate nonlinearity of the PZT scanner. The precision of this method depends strongly on the accurate parameter value. Although this method is difficult to obtain accurate values and is time consuming to identify the accurate parameters, it is widely applied in current commercial AFM systems for its low-cost and high image quality.

Another factor effecting the spatial uncertainties is the thermal drift. It is caused by the contraction and expansion of the AFM mechanical components due to the temperature changes[7]. The traditional solution generally costs a couple hours for scanning before manipulation to eliminate the drift influence aroused by the mechanical change in size. At the same time, AFM manipulation is strictly controlled under the homogeneous environment conditions[10]. Also this method is inconvenient and inefficient, for the thermal drift is still unobservable and temporal variant as reported in [11]. Thus the compensation methods based on the Kalman filter[11] and the neural networks[12] etc. are proposed to estimate the thermal drift. The performance of these approaches depends largely on the accuracy of the model parameters used to compensate the thermal drift, while it is difficult to obtain the accurate parameters. Then Monte Carlo Localization (MCL) based compensation method is proposed. By using the tip as a sensor [7,13], it can reliably estimate the thermal drift inside an AFM even with highly unstructured samples.

These methods focus on predicting the thermal drift between the tip frame and the sample surface frame, then indirectly estimating the tip position. While the approach proposed here directly localizes the on-line tip position by intermittently observing the landmark in the sample surface (task frame), referring to the macro robotic localization[14, 15].

In this research, the control model of AFM tip is calibrated, and the output of the tip motion is linearized by using a stochastic motion model, which consists of three parts: the Prandtl-Ishlinskii (PI) based hysteretic compensation, the creep compensation and the thermal drift compensation. However, the tip motion model alone cannot meet the requirements of estimating the positions for a long time, because the uncertainties in the nano-environments will accumulate over time. Then a local scan based landmark observation is developed to improve the tip position accuracy. By observing the landmark such as nano-particle and using the tip motion control input, the tip position is updated optimally. Some calibration experiments are included in this paper to estimate the probabilistic parameters of the tip motion model and the observation model. And the simulations and corresponding experimental results are shown as follows to illustrate the validity of the proposed method. Next nano-manipulation results with the different accuracy of the tip position are contrasted for illustrating that this method can promote the efficiency of nano-manipulation. Then a pattern is constructed using nano-particles to show that this method can provide a great potential for fabricating the nanostructure and device. Furtherly, the main factors effecting nano-manipulation are discussed. Finally, the nanostructures with different nano-particles are built for illustrating the validity of the proposed method.

The main contents of the sections are as follows. The system framework is given in section II. The stochastic motion model of the AFM tip is described in section III. The algorithm implement including parameter calibrations of the motion and measurement models, and the tip positioning experiments results are introduced in section IV. In section V, nano-manipulations with different tip accuracy are performed to illustrate the importance of tip localization in maneuvering, and a nano-structure is constructed with the proposed method. In Section VI, the main factors in AFM tip based manipulation are analyzed. Finally, the conclusions are given in section VII.

II. The Proposed Framework of Tip Positioning Control

The tip positioning model is established in the new architecture, including a feedback control on the AFM tip motion during nano-manipulation (see Fig.1). The tip can perform long time imaging and manipulation, if it is worn and dirty, the user can find this problem to change the tip for continuing the task.

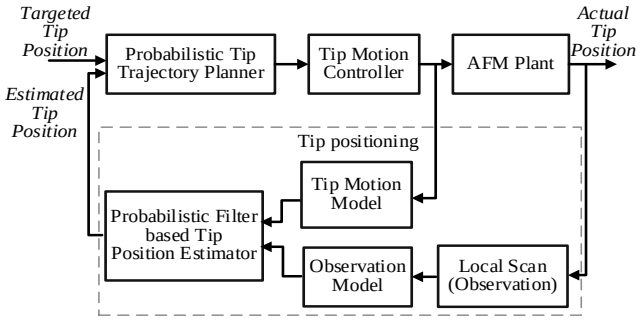

Fig.1. The architecture of the tip positioning control performing a nano-manipulation task.

This control module distinguishes from general feedback control systems[6, 16-22] in two points. First, two types of data are incorporated in the feedback loop: the motion estimation data and the observation data based on the local scan. The procedure of the local scan is shown in Fig.2 and described in the following B section. Feedback loop associated with tip position estimation using motion model can be performed at higher frequency, but the uncertainty of the tip position distribution will also increase with accumulation of estimating procedure. By using probabilistic filter with the higher accuracy, the landmark observation in feedback loop can update the tip position. But for the local scan actions, this updating process can only be executed in a lower frequency. Second, a probabilistic trajectory planner is included into the control loop for planning one or more local scan trajectories before a motion to the final target for manipulation.

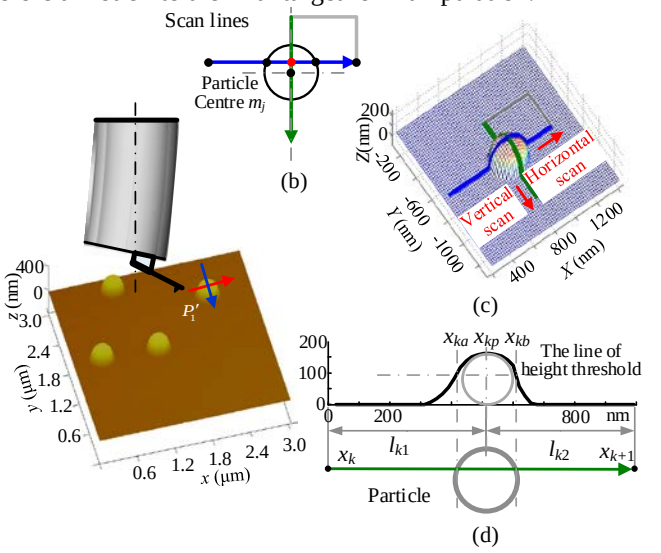

Fig.2. The proposed framework of tip positioning model (a) The nano-particle is observed using the local scan. (b) The local scan trajectory including horizontal and vertical scan is planned. (c) The local scan trajectory shown in 3D (d). The horizontal scan is shown for estimating x_{kp} by using Kalman filter in the following section II-*B*.

A. Tip Motion Model

The AFM tip position will be denoted by a two-dimensional vector x in the task frame. The state variable x_k denotes the tip position at discrete time k, X_k denotes the sequence of the tip positions or its path from time 0 to time k.

$$X_k = \{x_0, x_1, x_2, ..., x_k\} \tag{1}$$

Tip motion control data is denoted by u_k which corresponds to the motion of tip position from time k to time k+1. The sequence of control inputs is as follows:

$$x_{k+1} = g(x_k, u_k) + w_{k+1} \quad w_{k+1} \sim N(0, R_{k+1}) \tag{2}$$

where g(*,*) is the state transition function, w_{k+1} denotes error random variable with the distribution of the tip position, R_{k+1} is a 2-by-2 covariance matrix of the distribution. g (*,*) mainly depends on the tip previous position x_k and motion control u_k.

Additionally, PZT creep displacement effect d_k and system thermal drift $v_k*\Delta t$ are added for correcting the tip motion.

$$g(x_k, u_k) = x_k + u_k + d_k + v_k * \Delta t \tag{3}$$

where v_k is the thermal drift velocity vector, Δt is the time period from x_k to x_{k+1}. Since the motion tip is limited in a small area around the PZT centre, v_k, d_k, u_k can be assumed to be independent from each other when scanning and manipulating. These factors are different features of AFM components, and can lead into the tip uncertainties in the task space, so some methods should be adopted to compensate the tip uncertainties [6,11]. Accordingly, w_{k+1} mainly depends on the tip position distribution w_k at the state x_k, the linear superposition of three parts of the errors of u_k, d_k and v_k. The three random variables are considered to be with zero-mean Gaussian according to the calibration experiments represented in Section IV.

B. Landmark Observation based Positioning

During the horizontal and vertical scanning in Fig.2, the tip position is updated by using Kalman filter as following.

First, the tip position is optimally estimated at x_{kp} by using Kalman filter. Because the tip is used as a sensor to observe the landmark in the observation, this algorithm is different from the macro robot localization using other sensors to estimate the robot position.

The horizontal scan from x_k to x_{k+1} including the tip translation and the observation estimation at x_{kp} is analyzed as following. The tip translation from x_{kp} to x_{k+1} is expressed by the tip motion equation:

$$\hat{x}(kp \mid k) = x_k + l_{k1}^* \frac{x_{k,kp}^*}{\left\| x_{k,kp}^* \right\|} + w_{kp} \quad w_{kp} \sim N(0, R_{kp}) \tag{4}$$

where l_{k1} is a scalar variable, which denote the scan length (tip motion control) from x_k to x_{kp} in the scan profile in Fig.2, l_{k1}^* is the mean of l_{k1}, $x_{k,\,kp}$ is a random variable vector from x_k to x_{kp}, and $\| x_{k,kp}^* \|$ is the norm of the mean value of $x_{k,kp}$, i.e. l_{k1}. $x_{k,kp}^* / \| x_{k,kp}^* \|$ denotes the unit vector in the direction of the local scan in the task frame. w_{kp} is an error random variable which is the linear superposition of the error random variable w_k at x_k, and w_{k1} resulting from motion x_k to x_{kp}.

The observation estimation assumes that the observational point (x_{kp}) of the scan trajectory is the same position ($m_{j,xy}$) of the particle centre in the task frame. The $m_{j,xy}$ can be calculated according to Ref.[24]. The observation equation is as following:

$$\begin{aligned} z_{kp} &= h(x_{kp}, m_j) + v_{z,kp} \\ v_{z,kp} &\sim N(0, Q_{z,kp}) \end{aligned} \tag{5}$$

where z_{kp} is the observation value at x_{kp}, $v_{z,kp}$ is the random variable with Gaussian distribution. The uncertainties of local scan based observation mainly consists of three error sources that are independent mutually: the landmark position errors from the calculation in the map (v_{map}), errors of the different nano-particle centre on various local scan lines (v_{z_kl}) and errors from local scan direction deviation (v_{z_θ}) (these related information referred to the part: parameters calibration for observation model in the IV section). The combined random variable for these three errors is a linear superposition:

$$v_{z,kp} = v_{map} + v_{z\_kl} + v_{z\_\theta} \tag{6}$$

The real measure at x_{kp} is calculated as follows:

$$h(x_{kp}, m_j) = S_x m_j + S_y x_{kp} \tag{7}$$

where m_j is the landmark position. S_x and S_y are defined as selection matrix for the horizontal and vertical observation.

$$S_x = \begin{pmatrix} 1 & 0 \\ 0 & 0 \end{pmatrix}, \quad S_y = \begin{pmatrix} 0 & 0 \\ 0 & 1 \end{pmatrix} \tag{8}$$

In general, two non-parallel local scan actions are taken to fully observe the two-dimension position information in the task fame. These local scan actions take tens of milliseconds, and can be used to update the tip position in real time.

C. Tip Position Updation

The tip position is measured through the motion model and the observation model abovementioned. Then the tip optimal position at x_{kp} is estimated using Kalman filter.

III. A Probabilistic Motion Control of AFM Tip

During nano-manipulation, the PZT input voltage changes at the same rate, and the tip is controlled laterally step by step at a fixed interval. As the tip moves to a certain sample point after taking a fixed step along the scanning line, the height at that position is measured. Thus the scan profile could be obtained, then it will be used as 'a ruler' to measure the spatial distance between the tip and the feature. The tip motion model is also the foundation of the feature observation model. In the experiment, the fixed step is called as basic step, which is the smallest unit for the motion and the observation. The tip motion model includes three models: the PI model, the creep model and the improved thermal drift model. Additionally, an observation model is added in section IV. The establishments of these motion models are introduced below.

A. The PI and Creep Compensation Models for the PZT

As for the PZT material, the PI model is widely used to build the forward feedback controller to predict the tip position. The details of this model are represented in [9, 11, 23]. When the input voltage changes at the same rate, the displacement of the PZT is not only in relation to the current voltage, but also to the historical voltage. When the input voltage is a fixed value, the displacement will increase over a period of time, then reach a stable value. This transition procedure is called as the creep effect. We can build the creep model to express the transition state for increasing the accuracy in the tip positioning. The PI and creep models are described in [24].

B. The Thermal Drift Model

The thermal drifts in *x* and *y* directions can cause the change of the scanning interval distance between P_1 and P_2 in the multiple continuous images (see Fig.3). These images are continuously obtained by alternate scanning mode of frame up and frame down. The drift velocity is estimated by the following strategy.

The nano-particles in the images drift upward and rightward (see Fig.3). The image is obtained by scanning the sample line by line. As for each line, the tip scans from left to right. During

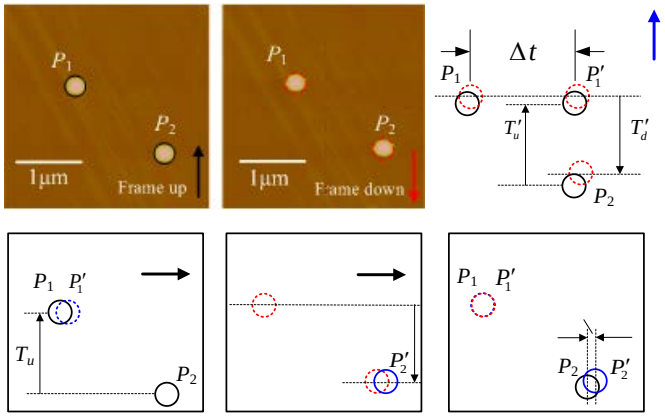

Fig.3. The drift velocities are calculated according to the change of the scanning interval distance and the time from P_1 to P_2 in the two continuous images. (a) and (b) show the continuous images of the nano-particle with the scan size 3.16μm, scan angle 0°, and scan rate 1.51 Hz. The thermal drift leads to the change of the interval distance between P_1 and P_2 in an image of frame up and a successive image of frame down in (c). (d) – (f) present the calculation of the horizontal drift velocity.

imaging procedure in frame up mode, P_2 is scanned first, then P_1 drifting far away from P_2 before P_1 is scanned. Thus the vertical scanning interval distance between P_1 and P_2 will become larger than their actual interval distance, which is denoted by d_{u_y}. While the vertical scanning interval distance will become smaller in the imaging procedure in frame down mode, which is denoted by d_{d_y}, for P_2 drifts toward P_1. The velocities such as v_{drift_x} and v_{drift_y} in x and y directions respectively are calculated as follows:

$$T_u' = T_u - \Delta t = \frac{d_y}{v_{scan\_y} - v_{drift\_y}} \tag{9}$$

$$T_d' = T_d + \Delta t = \frac{d_y}{v_{scan\_y} + v_{drift\_y}} \tag{10}$$

$$\frac{v_{scan\_y} + v_{drift\_y}}{v_{scan\_y} - v_{drift\_y}} = \frac{T_u - \Delta t}{T_d + \Delta t} \tag{11}$$

$$v_{drift\_y} = \frac{d_{u\_y} - d_{d\_y} + 2*\Delta t * v_{scan\_y}}{T_u + T_d} \tag{12}$$

$$v_{drift\_x} = \frac{d_{d\_x} - d_{u\_x}}{T_u + T_d} \tag{13}$$

where T_u' is the scanning time interval from P_2 to P_1 in frame up mode, its value is T_u minus Δt. T_u is the scanning time interval from P_2 to the assumed nano-particle P_1' which is on the right side of P_1. Δt is the additional time interval for finding P_1' from P_1 to P_1' in the horizontal scanning. T_d' is the scanning time interval from P_1 to P_2 in frame down mode, its value is T_d plus Δt. T_d is the scanning time interval from P_1' to P_2. Eq.11 is obtained by Eq.9 dividing Eq.10, then Eq.11 is transformed to Eq.12 to estimate the thermal drift in the vertical direction. As for the horizontal thermal drift, Eq.13 can be obtained similarly.

IV. Implementation of Positioning Tip

The model parameters of the motion and observation are calibrated for the PZT without sensor based control. And the simulation and the corresponding experimental results verify the algorithm.

A. Motion and Observation Models with Stochastic Calibration

i. Parameters Calibration for Motion Model

The tip motion model is expressed by Eq.2, the corresponding error random variable w_{k+1} is:

$$w_{k+1} = w_{k\_h} + w_{k\_c} + w_{k\_d} \tag{14}$$

where w_{k_h} is the error from the PI based motion model, w_{k_c} is the error from the creep model and w_{k_d} is the error from the thermal drift model.

(1) *The Parameters Calibration for the PI Based Model and Creep Model*

The parameters for the PI based motion model and the creep model in horizontal and vertical directions are calibrated separately by fitting the sample points of the hysteretic loop using the least square method. These sample points are obtained by making dents on compact disk (CD) surface, which are used to calibrate the model parameter. The calibration procedure is described in [24].

(2) *The Parameters Calibration for the Thermal Drift Model*

The velocity of thermal drift is calculated using several groups of continuous images, which are obtained in several days. The velocities of thermal drift are estimated. And it is found that the velocities fluctuate around a value after the AFM system runs 2~3 hours and reaches its stability. The thermal drift velocities are fitted with Gauss function, the results are as following: μ_x = -0.004nm/s, σ_x = 0.027nm/s, μ_y = 0.099nm/s and σ_y = 0.209 nm/s. The mean of the velocities in x direction is closer to zero. The mean in y direction is closer to a positive value.

ii. Parameters Calibration for Observation Model

The nano-particle centre x_{kp} is observed to estimate the tip position, the sensing errors mainly come from three parts:

$$v_{map} \sim N(0, Q_{map}) \quad v_{z\_kl} \sim N(0, Q_{z\_kl}) \quad v_\theta \sim N(d_\theta, Q_\theta)$$

(1) *The Error v_{map} of The Nano-particle Centre in the Pre-image*

The task frame is set up in the target region of the sample surface where the features such as nano-particles are presented by using the pre-image. The nano-particle centre calculation is effected due to nonlinearity of the scanner lateral displacement and the thermal drifter. The uncertainties of the nano-particle centre are stochastically calculated by localizing the same nano-particles on multiple scanning images repeatedly. First, multiple images of the same region (with the same nano-particles) are obtained. Second, the differences of the height reference among the multiple images are compensated according to the top height of the nano-particle P_1. The top height is the mean of the neighborhoods points (nine points) around the top point. Third, the nano-particle P_2 centre relative to the centre of the nano-particle P_1 is calculated, and is found

to obey Gaussian distribution according to the fitting results: μ_x = 0.0 nm, σ_x = 5.0 nm, μ_y = 0.0 nm and σ_y = 4.5 nm.

(2) *The Error v_{z_kl} of Nano-particle Centre due to Local Scanning the Different Part of the Nano-particle*

The measurement of the nano-particle centre is also disturbed by scanning the different part of the nano-particle. The measurement model may perform different scanning along line 1, line 2, or other line as shown in Fig.4(a). The nano-particle centre x_{kp} may be stochastically calculated by calculating the different scanning line around the nano-particle in the pre-image, and the distribution subjects to the Gaussian distribution with μ_y = 0.0 nm and σ_y = 4.7 nm.

(3) *The Error v_θ of Nano-particle Centre due to the Deviation of the Local Scan Angle*

Here the deflection of the real scanning line is caused by the creep effect and the construction of the PZT scanner. Fig.4(b) shows that the deflection angle θ between the real scanning line and idea line is stochastically calculated through multiple scan lines which are recorded by punching the dents at the two ends. θ is smaller than 1°, and regarded to be disturbed by Gaussian noise with the covariance: 0.39°. d_{kp} is the distance between the nano-particle centre and the scanning line. If the d_{kp} equals to the extreme value, i.e the nano-particle radius, the maximum of the nano-particle centre deflection d_θ is close to 2nm. Thus v_θ can be neglected in the observation model.

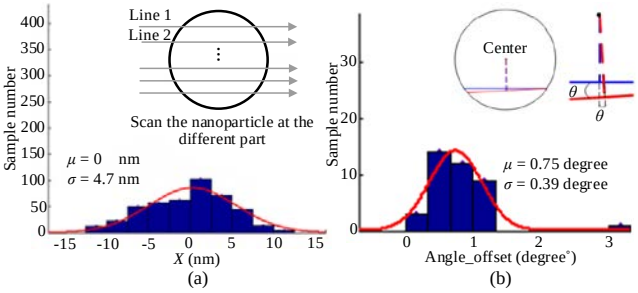

Fig.4. The error distribution of the nano-particle center is induced by local scanning the different part of the nano-particle in (a) and the deviation of the local scan angle in (b).

B. Simulation and Experimental Results

To illustrate the validity of the abovementioned method, the related simulation and experiment are designed and performed with veeco Dimension 3100. The parameters of motion model of AFM tip are obtained from calibration experiments. The parameters of observation model are calibrated by repeatedly scanning the same area as abovementioned.

In the experiments, multiple polystyrene nano-particles with the diameter about 200nm are scattered on the CD substrate. An area including at least one nano-particle is selected and pre-imaged. Then imaging is stopped and the tip is moved to the centre of the scanning region. Next, the tip is moved to x_0 stochastically with the same distribution for each experiment. This procedure is as following: first, moves the AFM tip from the centre to x_2; second, performs local-scan based localization along the path $x_2 \rightarrow x_3 \rightarrow \cdots \rightarrow x_6$; third, updates the tip position x_6, plan and move the tip to x_8 with high accuracy along the path $x_6 \rightarrow x_7 \rightarrow x_8$; Finally, moves the tip to x_0 along the path $x_8 \rightarrow x_{d\_1} \rightarrow x_0$ (marked by the dotted line in Fig.5) and punches the dent at x_0. Due to the long moving distance from x_8, the uncertainties of the tip position at x_0 will increase. Thus the tip moves to x_8 using local scan method and punches for recording its localized position. The tip positioning experiments are performed 50 times, the distribution of tip position on waypoints is shown in Fig.5(a) and (b).

The tip observes the landmark 2 times, which include a horizontal measurement (for x_2 to x_3) and a vertical measurement from x_5 to x_6. The tip performs positioning control in the horizontal component of position after horizontal observation. And the accuracy of the horizontal component of x_4 or its later position can be statistically estimated. Likewise, the tip can calculate the accuracy of vertical component of x_7 or its later position after vertical observation. The experiment of localizing the tip using landmark observation includes multiple positions. Some positons such as x_0, x_2, x_5, x_6 and x_8 are used as key positions in the Table 1 for representing the localization procedure. And other positons such as x_1, x_3, x_4, x_7 as the way points are neglected. Table 1 first lists the distribution of the initial position x_0. When the tip moves to x_3 after horizontal observation, the positioning control in the horizontal component is performed at x_5, then the tip moves from x_5 to x_6 for estimating the tip position in the vertical direction. x_5, x_6 distribution are listed including u_x, σ_x in the Table 1. While u_y, σ_y are not counted because there is not any control in the vertical component. Then the positioning control is added in the vertical direction in x_7 and x_8. The x_8 distribution in the Table 1

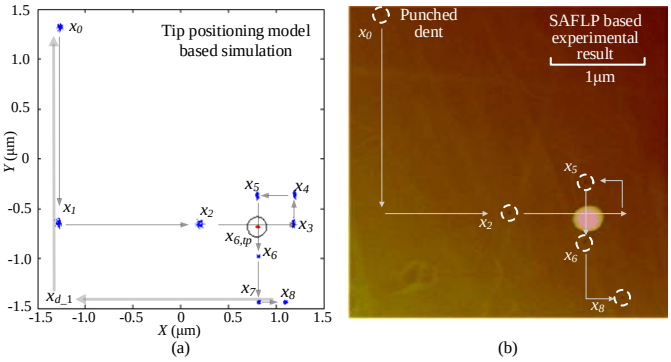

Fig.5. The tip is moved from x_0 to x_8 by using the proposed algorithm. The tip positions at x_0, x_8 and the waypoints are recorded by punching the dents. Scanning image shows that these punched dents in the white dash line circles marks the tip positions in the different waypoints. 50 experiments have been performed.

Table.1 Simulation and experimental results of positioning the tip by using the proposed method. (μm)

	Simulation data				Exeprimental data			
	μ_x	μ_y	σ_x	σ_y	μ_x	μ_y	σ_x	σ_y
x_0	-1.245	1.316	0.013	0.016	-1.319	1.474	0.015	0.019
x_2	0.239	-0.700	0.016	0.020	-0.009	-0.599	0.017	0.022
x_5	0.804	-0.371	0.008	0.020	0.792		0.006	
x_6	0.764	-0.985	0.008	0.006	0.783		0.010	
x_8	1.101	-1.471	0.009	0.008	1.178	-1.495	0.010	0.007

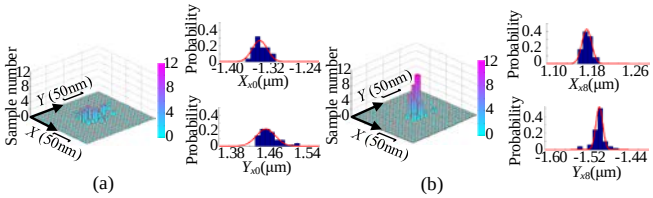

Fig.6. Gaussian fitted results for the tip distribution at x_0 and x_8 in local scan based moving. (a) and (b) are the distributions zoomed in at x_0 and x_8. Two figures on the right of (a) are the fitted curves for the distributions in x and y directions at x_0, respectively. Two figures on the right of (b) are the fitted curves for the distributions in x and y directions at x_8, respectively.

is estimated. Additionally, these positions from x_0 to x_8 are defined in the task space, and cannot be detected by any sensor directly. We obtained these positions through punching dents on the CD surface, rescanning these regions, and calculating the dent positions in the rescanning image. In order to get the position distribution, we performed 50 experiments. Considering the tip maybe be broken in punching the dents, we need not record all of the positions for reducing the punch times. Fig.6 shows the experimental results in the 3D histogram, the Gaussian fitted curves for the distributions in X, and Y directions at start position x_0 and target position x_8. The tip moves from x_0 to x_8, its uncertainties will increase if using the traditional approach. Therefore, we propose landmark observation for improving accuracy of the tip position. The accuracy of x_8 distribution is estimated to contrast its value with x_0 distribution for illustrating validity of the proposed method.

V. Validation of the Proposed Method in Nano-manipulations

The tip lateral position related to the nano-particle plays an important role when maneuvering the nano-particle. In this paper, a landmark observation strategy is proposed to improve the tip position accuracy, and then promote the efficiency of nano-manipulation. Following experiments will validate this method using the statistical techniques. The different accuracies of the tip position relative to the same nano-particle are quantitatively obtained through resampled 50 experimental positions. These positions are consisting of the localized positions of the tip through observing the nano-partilce and other several groups of the intended uncertainty positions, all of which come from 190 times of repetitive experimental nano-manipulations. The corresponding nano-manipulation results are contrasted to illustrate the influence of the tip accuracy on the manipulation. And a nano-structure is assembled using the proposed method.

A. Statistic Experiment Design for Demonstrating the Proposed Method

The experimental details are described as follows: the tip is firstly positioned on the image centre, then moved to P_l through local scan based observation with high position accuracy (see Fig.7(e)). Next the tip is moved to the idea position P_s for pushing the nano-particle from P_s to P_t along maneuvering direction l through the nano-particle centre. The maneuvered position is near to the expectable position as shown in Fig.7(*f*). If the tip is positioned without using the proposed method, the start position may be on the position P'_s (below P_s) or P''_s (above P_s), this will lead to an uncertainty error in nano-manipulation, as shown in Fig.7(*a*) (*i*). The experimental procedure simulates the tip position errors caused by the system uncertainties by moving the tip to positions P'_s and P''_s after accurately estimating the tip position at P_l with local scan method. The perpendicular distance between the tip simulated uncertainty position and the expectable path l is denoted as d. With d increasing, the uncertainty for nano-maneuvering becomes larger. The experimental results are analyzed in following *B* parts.

B. Analysis of the Experimental Results

Experiment results in Fig.7 clearly show the tendency of the influence for the tip position uncertainty on nano-manipulation. To quantitatively express the relationship between the tip position uncertainty and the performance of nano-manipulation, the resampling technique with replacement is adopted to represent the different tip distributions. By using 13 groups of experiments data with various uncertainty positions (see Fig.8), 6 group of distributions of tip positions are generated. For simulating the distribution i, several classes of the uncertainty positions with offset d sets [0, ±20*i] (i =1,…,6) are resampled with N_s times respectively (see Table 2.). These distributions are defined in F_{Rot45} frame (see Fig.8 (b), (c)) for easier reading. The tip standard deviations at P_s are with σ_x = ~3.0 nm, σ_y = ~3.0 nm after the local scan based observation (if the tip is moved directly to P_s from the image centre without observation, the standard deviations are with σ_x = ~5.0nm, σ_y =~5.0nm). This frame is originated at the nano-article centre P_O. These

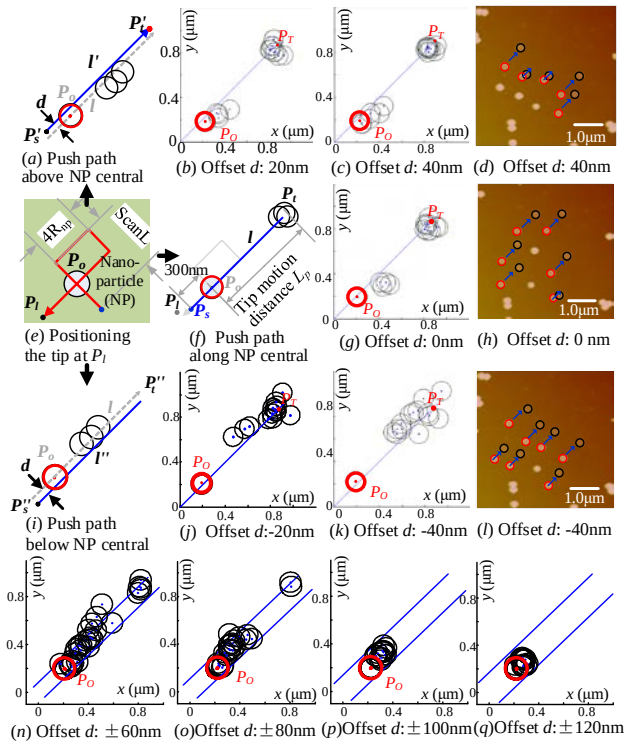

Fig.7. The experimental diagrams show that the tip uncertainties can seriously affect the efficiency of nano-manipulation. The experiments data are divided into 13 groups with offset d =0, ±20nm, ±40nm, ±60nm, ±80nm, ±100nm, ±120nm.These figures can be divided into two parts. one part of (*a*), (*e*), (*f*) and (*i*) illustrates how to simulate the tip position uncertainties. (*e*) shows that the tip is first accurately positioned at P_l by using the local scan method. The scan length ScanL is 500nm. The nano-particle (NP) radius is 90nm, and the tip radius is 20nm. (*f*) shows that the tip is moved to position P_s for pushing the nanoparticle. (*a*) illustrates that the tip uncertainties are simulated in the case of positioning the tip at P'_s with push path above NP central. (*i*) similarly represent that the tip is positioned at P''_s for simulating its uncertainties with push path below NP central. The other part consists of the remaining figures which shows the experiments results according to abovementioned simulation plan. (*b*) and (*j*) separately represent the manipulation results when the push direction is not through the nanoparticle centre P_o (the offset d = ±20nm). (*c*) and (*k*) shows the experimental results with the offset d = ±40nm. (*g*) is the manipulation result with the offset d = 0nm, which is used for comparing with other results of offset | d | >0 nm. (*d*), (*h*) and (*l*) are used for representing the experimental result for statistical chart (*c*), (*g*) and (*k*) respectively. (*n*) ~ (*q*) show the other statistical results with offset distance d: ±60nm, ±80nm, ±100nm, ±120nm respectively.

simulated distributions from 1 to 6 at P_s become larger mainly in the *y* direction and remain the same degree in the *x* direction in F_{Rot45} frame. And these distributions are fitted by using Gaussian distribution in Fig.8. The corresponding parameters and manipulation results are shown in Table 3. In Table 3, *m* direction represents the manipulation direction, and *v* direction represents the direction vertical to *m* direction. μ_m is the tip position mean at P_s in *m* direction, σ_m is the standard deviation for μ_m, μ_v is the tip position mean at P_s in *v* direction, σ_v is the standard deviation for μ_v. N_{suc} is the count of successful nano-manipulations when the maneuvered nano-particle positions fall into the rectangle region (according to 3σ principle) in *m* direction and *v* direction (see Fig.9). μ_{suc} is the mean distance of the successful manipulations in *m* direction. Correspondingly, μ_{lost} is the mean distance of the unsuccessful manipulations in *m* direction, and decreases from 464.2nm to 286.9nm. The successful manipulation case N_{suc} decreases from 35 to 16 in 50 experiments with the distribution becoming larger. Additionally, the error standard deviation in *v* direction is estimated by counting all the data from distribution 1 to distribution 6. The relation between the tip manipulation distance and the tip motion distance in *m* direction is calibrated by using a series of tip motion distances L_p. The experiment for each L_p includes multiple times of manipulation. The experimental data about the manipulation distances in *m* direction are shown in Fig.10(a). The red line is fitted by using Random Sample Consensus(RANSAC) algorithm [26], and the outliers (red points) are excluded. Fig.10(b) shows the corresponding distance error model, which is obtained by calculating the standard deviations σ_{mp}. The standard deviation σ_{vp} of the manipulated nano-particle in *v* direction is calculated by using all the data. The successful region is defined by using a rectangle with width $6*\sigma_{mp}$ and height: $6*\sigma_{vp}$ (see Fig.9). As shown in Fig.9, the lost nano-particle centre (blue bars) isgradually close to the start point P_o with the uncertainty of the AFM tip increasing. This is not just verifying our common conclusion of single tip manipulation with unstable results, but also providing quantitative results for analyzing the relation

Offset / Resampling	Offset: *d* (nm)												
	-120	-100	-80	-60	-40	-20	0	20	40	60	80	100	120
Distribution 1	0	0	0	0	3	14	16	14	3	0	0	0	0
Distribution 2	0	0	0	1	5	12	14	12	5	1	0	0	0
Distribution 3	0	0	1	3	5	10	12	10	5	3	1	0	0
Distribution 4	0	1	2	3	6	8	10	8	6	3	2	1	0
Distribution 5	1	2	3	4	5	6	8	6	5	4	3	2	1
Distribution 6	1	3	4	4	5	5	6	5	5	4	4	3	1

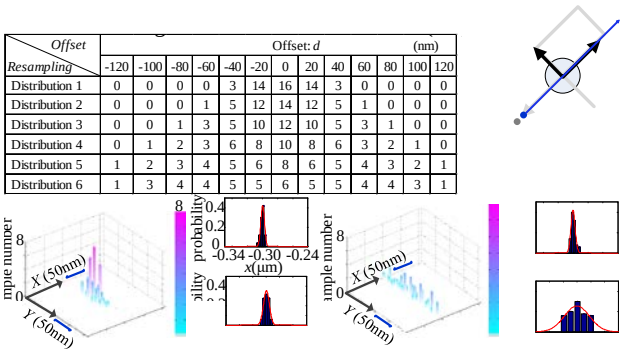

Fig.8. (a) ~ (c) show 1th and 6th distribution images at P_s defined in F_{rot45} coordination respectively for analyzing nano-manipulation results. The uncertainty distributions are constructed by resampling from 13 groups data. These groups of experimental positions with different *d* are used to simulate the tip distribution 1 - 6 with 50 samples. Table 2 shows how to constitute the uncertainty distributions. N_s is resampling times from certain groups of uncertainty positions for forming the simulated distributions. The manipulation results of these samples are used to analyze the influence of the tip uncertainties on the manipulation. (a) shows that these distributions are made up in the frame F_{rot45} for easier reading.

Table3.The different distributions and their corresponding results (nm)

	μ_m	σ_m	μ_v	σ_v	N_{suc}	μ_{suc}	μ_{lost}
Distribution 1	-299.7	2.4	2.0	21.8	35.0	912.2	464.2
Distribution 2	-300.4	2.0	-1.5	36.5	33.0	902.1	364.4
Distribution 3	-299.9	2.1	-1.9	41.0	31.0	914.8	269.2
Distribution 4	-299.6	3.5	5.1	47.1	26.0	914.7	360.1
Distribution 5	-299.9	2.7	0.2	60.4	18.0	924.9	328.8
Distribution 6	-300.0	2.9	0.4	91.2	16.0	911.2	286.9

between the uncertainty of the tip position and the particle lost. During nano-manipulation, the tip is used to observe the manipulated object position in horizontal and vertical direction (see Fig.11). Due to the tip position uncertainties, the tip should avoid contacting the nano-particle at the waypoints such as x_k, x_{k+1}, x_{k+3} and x_{k+4}.These ellipse bounders are contained in the certain region with definite width and height. This certain region can be used to estimate the number of features to be assembled per unit length.

C. Proposed Method based Manipulation for a Structure Assembly

A nano-structure is assembled by using the proposed method. This structure is the normal heptagon whose circum-circle radius is 1.7μm. Fig.12(a) shows that nano-partilces P_1—P_7 are autonomously pushed to the target positions around P_0. Fig.12(b) presents that the nano-particles P_1~P_7 are configured to construct the pattern. During the manipulation, the nano-particle may be left on the pushing trajectory because the stability for single tip pushing is limited. This problem can be solved partially by repeating the local-scan and particle pushing operation since the proposed method is feasible to run autonomously. In the experiment, the whole algorithm runs in a loop with two terminal conditions. First, the estimated distance from the nano-particle to the target position is smaller than 60 nm. Second, the local-scan and particle-pushing operations for each particle should be performed no more than 3 times. Fig.12(c) shows that another normal heptagon is constructed on the right of the first heptagon via the same steps. This result shows that the proposed approach has high potential for nano-manipulation in nano-manufacturing, especially by incorporating nano-hand approach [27-28].

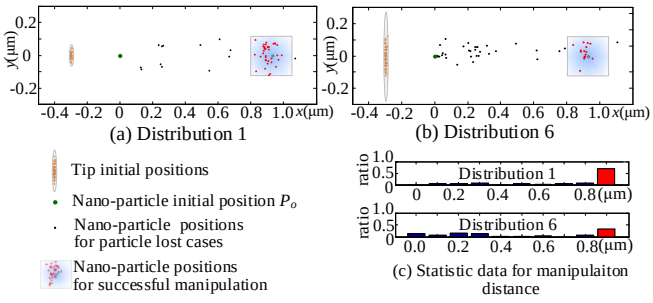

Fig.9. The manipulation results for 6 different distributions at P_s.

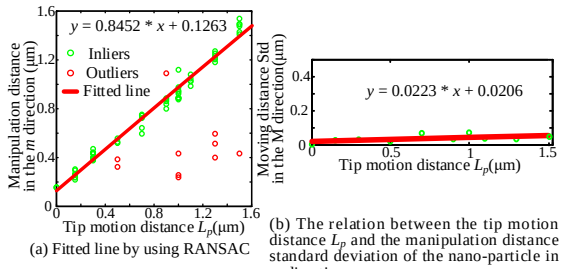

Fig.10. The relation between the tip motion distance L_p and the manipulation distance of the nano-particle in m direction.

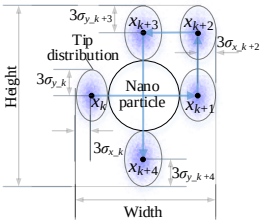

Fig.11 The region for observing the nano-particle. We can define the tip distribution region as an ellipse according to 3 sigma rule. The tip distribution bounder is adjoined to the nano-particle bounder to avoid the tip contacting the nano-particle at the waypoints, and to make sure that the distance between the tip and the nano-particle is the shortest.

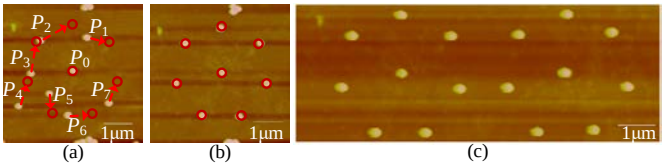

(a) (b) (c)

Fig.12. The region with several nano-particles is found to assembly a designed structure. (a) Initial image is scanned for the region. (b) Nano-particles are moved to construct a normal heptagon whose edge number is seven and circle radius is 1.7μm. (c) The constructed pattern includes two normal polygons with seven edges each.

VI. Analysis of Important Factors in AFM Tip Based Nano-Maniplation

The main factors in AFM tip based nano-manipulation are furtherly studied, which includes the landmark domain, the contact characteristics between the nano-particle and the substrate, and the tip shape. Furtherly the experimental results are provided to illustrate the efficiency of the proposed method.

A. Assurance of the Tip Position Accuracy in the Landmark Domain.

After localizing around the landmark, the tip is moved to the push position. Then the region around the push position is defined for guaranteeing the tip position accuracy, and the landmark is required within this region, which can be estimated according to the precision requirement at the push position and the tip localization accuracy around the landmark.

The landmark domain is calculated by the following formula. Assuming that the tip localization accuracy (Var (P_l), Var () is a function to fetch the variance of the tip position error) around the landmark and the precision allowance (Var (P_t)) at the push position are known in advance, the tip translation ($d_{l,t}$) from P_l should meet the following restraint condition:

$$Var(\, d_{l,t}\,) + Var(\, P_l\,) = Var(P_t\,) \qquad (15)$$

where $d_{l,t}$ is the translation path from P_l to P_t. The tip motion uncertainties variance Var ($d_{l,t}$) increase linearly with the translation $d_{l,t}$. Var ($d_{l,t}$) can be calculated by using the tip motion model. The tip moves along the horizontal or vertical direction step by step in the any translation path as shown in Fig. 13 (a) and (b). After observing the nano-particle, the tip is localized around this nano-particle. To simplify the analysis of the landmark domain, the tip is assumed to be localized around the nano-particle centre with the radius distance ($R_{n,t}$) of the nano-particle radius and the tip radius in Fig.13 (c). This localized position can guarantee the high localization accuracy and avoid the collision between the nano-particle and the tip. Furthermore, these localizations can be regarded as similarly

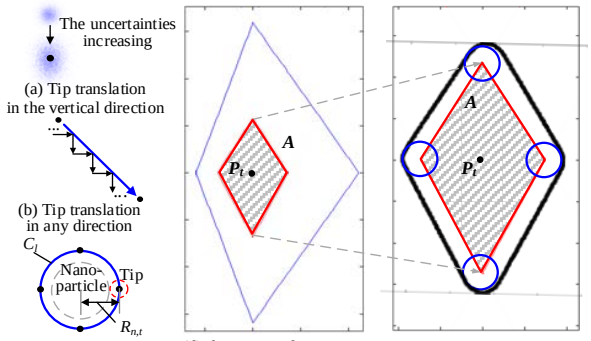

Fig. 13 The tip translation and localization and the simulation in the landmark domain of the target position.

forming a circle shape (C_l) around the nano-particle with the same accuracy (Var (P_l)). The circle radius equals to $R_{n,t}$.

The push position (P_t) is assumed as the original point (0,0) in the task space, as shown in Fig.13(d). The landmark domain boundary around P_t in Fig.13(d) is calculated according to Eq.15 by using the relation between the tip translation distance and its position variance in the tip motion model. Eq.15 can be transformed to Eq.16 and Eq.17 according to the restraint condition of the horizontal variance and the vertical variance at position P_t respectively. Var_x (*) and Var_y (*) are used to calculate the variance at a certain position or caused by the translation. In our studies, the variance at P_l is set to ([5nm]^2, [5nm]^2), the variance at P_t is set to ([10nm]^2, [10nm]^2), the variance for the translation $d_{l,t}$ is calculated through the motion model.

$$Var\_x(\, d_{l,t}\,) + Var\_x(\, P_l\,) = Var\_x(P_t\,) \qquad (16)$$

$$Var\_y(\, d_{l,t}\,) + Var\_y(\, P_l\,) = Var\_y(P_t\,) \qquad (17)$$

The outer polygon in Fig.13(d) is calculated according to Eq.16, the inner polygon is calculated according to Eq.17. The intersection (A) of the two polygons is the constraint border of the tip localization (P_l). The landmark domain (outer border) in Fig.13 (e) is calculated using the dilation operation between A and C_l.

In the experiment, the nano-particle is used as the landmark for localizing the tip, and then the tip is used to push the nano-particle. To ensure the tip accuracy, the push position is set to 300nm away from the nano-particle centre along nano-manipulation direction. This push position is close to P_l, so the positioning accuracy approximates to the accuracy of P_l.

B. Analysis of Contact Characteristics between the Nano-particle and the Substrate

First, the tip is used to observe the nano-particle to localize the tip position, then the nano-particle is pushed at a constant velocity. We can detect the deflection signal variation including vertical and horizontal variation in the Position Sensitive Detector (PSD) in Fig.14(a). Next the push force is estimated using lateral deflection, at the same time the vertical deflection is detected during the manipulation as shown in Fig.14(b). The signal variations from start to finish are related to the push force during the manipulation, and the push direction is perpendicular to the cantilever direction. The deflection value in the lateral direction

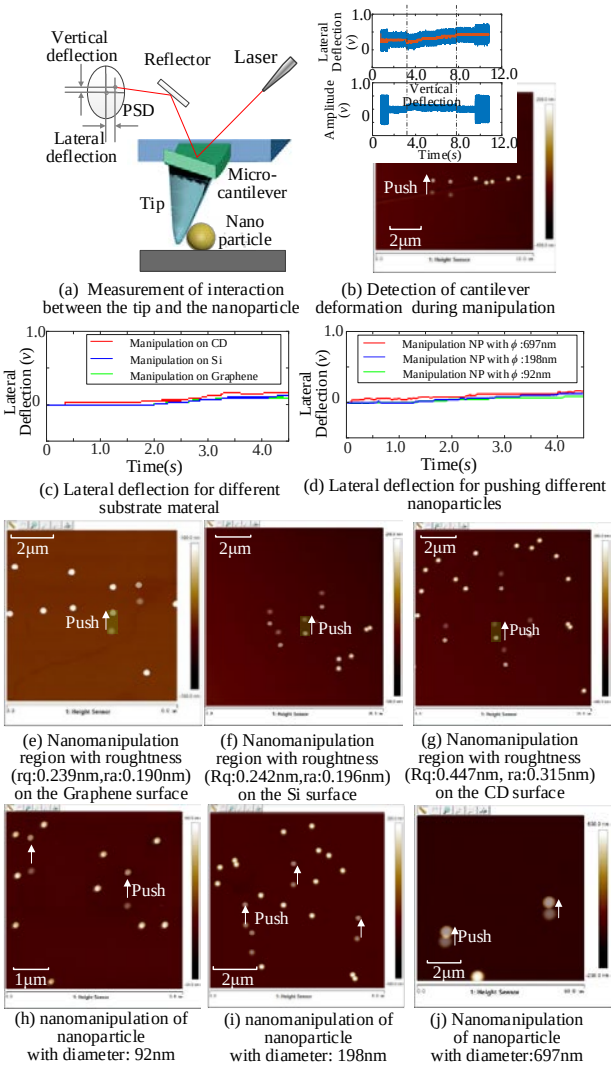

(a) Measurement of interaction between the tip and the nanoparticle

(b) Detection of cantilever deformation during manipulation

(c) Lateral deflection for different substrate materal

(d) Lateral deflection for pushing different nanoparticles

(e) Nanomanipulation region with roughtness (rq:0.239nm,ra:0.190nm) on the Graphene surface

(f) Nanomanipulation region with roughtness (Rq:0.242nm,ra:0.196nm) on the Si surface

(g) Nanomanipulation region with roughtness (Rq:0.447nm, ra:0.315nm) on the CD surface

(h) nanomanipulation of nanoparticle with diameter: 92nm

(i) nanomanipulation of nanoparticle with diameter: 198nm

(j) Nanomanipulation of nanoparticle with diameter:697nm

Fig.14 Nano-manipulation of the particles with different substrates and diameters. The method detects the push force variation when the same diameter nano-particle is manipulated on different substrate material, also the different diameter nano-particle is used to analyze the push force. According to the experiments from (e)-(j), we can conclude that the push force will increase with the substrate roughness becoming bigger, Similarly, the push force will increase with nano-particle diameter becoming larger, as shown in (c), (d).

represents the push force size. This method can be used to detect the push force variation when the same diameter polystyrene nano-particle is manipulated on the different substrate material, and the different diameter nano-particle is used to analyze the push force. According to the experiments from Fig.14(e)-(j), we can conclude that the push force will increase with the substrate roughness becoming bigger, Similarly, the push force will increase with the nano-particle diameter becoming larger, as shown in Fig.14(c), (d).

C. AFM Tip Shape Impact for Effective Nano-manipulation

The geometry of the cantilever and the tip shape has larger influence on the pushing operations as well as imaging [29, 30]. We have taken a picture of the tip as shown in Fig.15(a), as we know, the procedure of tip imaging can be regarded as dilation in the mathematical morphology, and we can estimate the tip shape by using the erosion operator. The tip shape is estimated by eroding the nano-particle image (see Fig.15(b)) which is the dilation of the tip shape on the sample surface. The tip shape can be estimated before nano-manipulation with easy preparing nano-particle sample, imaging and short time calculation in a few second. Four tip shape estimated results are obtained through eroding the images of the nanoparticles with diameters 92nm, 198nm, 462nm and 697nm (see Fig.15(c)), then their intersections are calculated (see Fig.15(d)). Next the front and side profiles of the tip shape estimation and the tip SEM image are contrasted to illustrate the method validity (see Fig.15(a)). After obtaining the shapes of the tip and the nano-particle, the action point is determined by calculating the minimum distance between the surfaces of the tip and the nano-particle. The contact plane is calculated by fitting the set of surface feature points in the neighborhood of the action point. The normal of this plane is the direction of the actual pushing force. Fig.16 (a) shows the contact push between the tip and the nano-particle in 3D. Fig.16(b) shows the intersection angle θ_{ia} between the push direction and the actual force direction with a certain tip offset. Fig. 16(c) illustrates that the tip offsets have important influence on the actual force direction when the tip is pushed upward vertically. Through some statistic experiments, the manipulation distance with different tip offsets is obtained to verify that influence shown on the left side of Fig. 16(c). On the right side of Fig. 16(c), the experimental images before and after the push operation are overlapped for calculating the manipulation distance. In Fig.16(d)-(h), the direction of the actual pushing force is calculated during the vertical push (S_1) with different tip offsets. Table 4 shows the intersection angle θ_{ia} which changes with the different tip offsets. When the offset is 0.01 μm, the push distance is maximum, while θ_{ia} is minimum. It is concluded that the effect of the tip shape on the pushing result becomes better as θ_{ia} becomes smaller.

During the manipulation, the direction of tip pushing is varied from 0° to 360°. In order to minimize θ_{ia}, it is necessary to perform fine-tuning of the tip offset position. This study mainly considers the tip position compensation from S_1 to S_8 for effective manipulation (see Fig.17). Fig.17(a) and (b) show that the tip offsets for S_1 and S_2 are calculated along the direction perpendicular to the manipulation direction. Fig.17(c) shows that the tip offsets from S_3 to S_8 will be compensated similar to S_2. Table 5 is the compensation results of the tip offsets for S_1 to S_8. The effectiveness of this method is furtherly illustrated by constructing the complex nano-structures. Finally, a string of "NanoLab" is constructed in the scanning image area with size 8μm, also the pixel resolution is 31nm, and the error threshold is defined as 60nm (see Fig.18). The average push times of 39 nano-particles is 2.3.

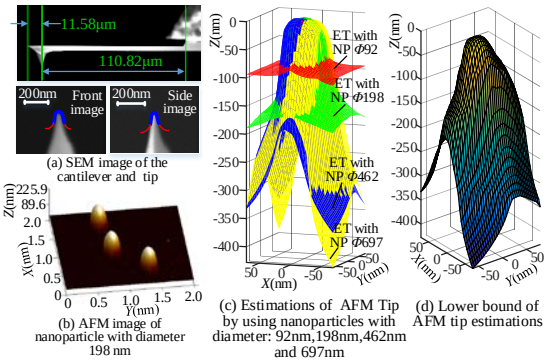

(a) SEM image of the cantilever and tip

(b) AFM image of nanoparticle with diameter 198 nm

(c) Estimations of AFM Tip by using nanoparticles with diameter: 92nm,198nm,462nm and 697nm

(d) Lower bound of AFM tip estimations

Fig.15 Estimation of the tip shape and validation of its results.

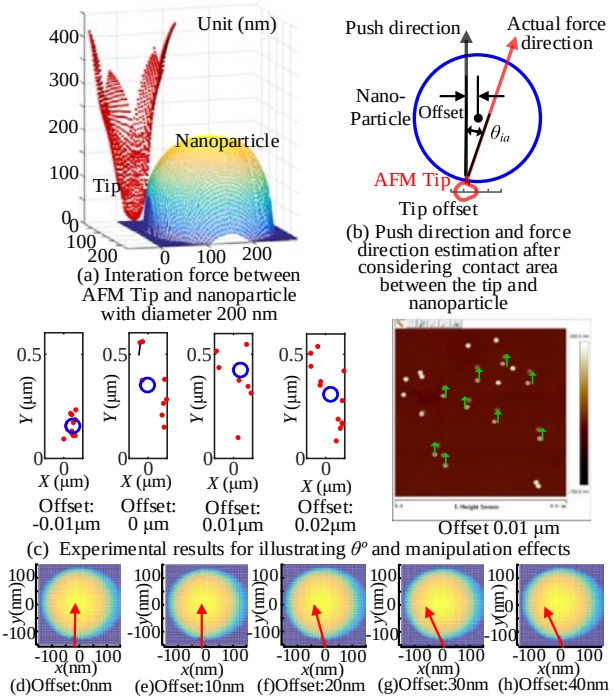

(a) Interation force between AFM Tip and nanoparticle with diameter 200 nm

(b) Push direction and force direction estimation after considering contact area between the tip and nanoparticle

(c) Experimental results for illustrating θ^o and manipulation effects

Fig.16 Tip position compensation for minimizing the intersection angle θ_{ia}.

Table 4. Intersection angles between the push direction and the force direction for different offsets from bottom to top.

	Offset								
	-40	-30	-20	-10	0	10	20	30	40
θ(°)	-15.36	-11.02	-9.50	-2.51	-0.80	**0.00**	14.79	18.24	16.63

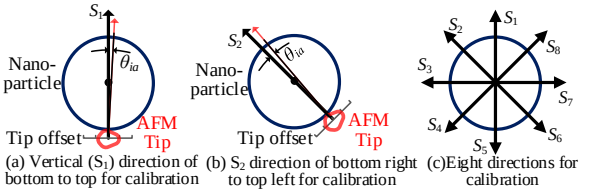

(a) Vertical (S_1) direction of bottom to top for calibration (b) S_2 direction of bottom right to top left for calibration (c)Eight directions for calibration

Fig. 17 Compensation of the tip offsets on the push directions from S_1 to S_8.

Table 5. Intersection angles θ_{ia} for different offsets from S_1 to S_8 (degree °).

	Offset (nm)								
	-40	-30	-20	-10	0	10	20	30	40
S_1	-15.36	-11.02	-9.50	-2.51	-0.80	**0.00**	14.79	18.24	16.63
S_2	-19.48	-18.89	-12.06	-9.56	-10.57	-4.46	**0.00**	0.44	6.08
S_3	-21.05	-13.72	-13.92	-11.50	-8.62	**-4.25**	5.38	10.14	7.54
S_4	4.65	3.58	6.27	**-1.81**	-4.62	-8.35	-13.96	-19.83	-17.82
S_5	15.90	12.69	11.14	4.94	2.59	**-1.23**	-3.00	-7.59	-9.85
S_6	20.03	12.09	6.95	2.44	**0.37**	-0.95	-5.06	-9.23	-6.65
S_7	24.20	19.77	8.45	9.22	8.27	**-0.68**	-2.78	-2.58	-7.52
S_8	12.92	12.59	7.16	4.17	**-0.29**	-2.58	-3.34	-8.12	-15.49

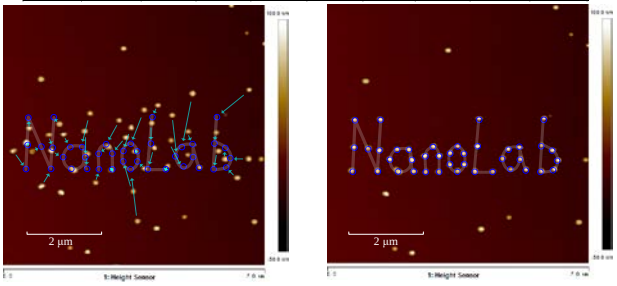

Fig.18 39 nano-particles with the initial and the target positions in the left image are manipulated to positions of "NanoLab" formation precisely in right image. Average manipulation times are 2.3 with the average distance: 0.510μm.

VII. Conclusions

The position uncertainties of the tip in the AFM Tip task space still exist due to the thermal drift, nonlinearity of the AFM scanner and other error sources. Therefore, a local scan based approach including the tip motion model and observation model is proposed for positioning the tip in nano-manipulations. The parameters of the observation model and the motion model are stochastically calibrated through the designed experiments. And the tip positioning importance is shown by contrasting nano-manipulation results with the different accuracy of the tip positions. The main factors including the landmark domain, contact characteristics between the tip and substrate, and tip position offset for compensating the tip shape effect are analyzed. Finally, the nano-structure with two polygons and a string "Nano Lab" is constructed by using the proposed method with about 2.3 manipulation times per nano-particle. The experimental results illustrate that the proposed approach can implement a fast and valid nano-manipulation, which provides the technological support for the nano-assembly automation in fabricating MEMS/NEMS device.

References

[1] H. Xie, C. Onal, S. Rgnier, and M. Sitti, *Atomic Force Microscopy Based Nanorobotics: Modelling, Simulation, Setup Building and Experiments*: Springer Publishing Company, Incorporated, 2011.

[2] K. M. Xu, A. Kalantari, X. P. Qian."Efficient AFM-Based Nanoparticle Manipu- lation Via Sequential Parallel Pushing," *IEEE T. Nanotechnol.*, vol.11, no.4, pp. 666-675, 2012.

[3] V. Chawda, M. K. O'Malley. "Vision-Based Force Sensing for Nanomanipulation, "*IEEE-ASME T. Mech.*, vol. 16, pp. 1177-1183, 2011.

[4] M. Sitti, and H. Hashimoto, "Controlled pushing of nanoparticles: modeling and experiments, " *IEEE-ASME T. Mech.*, vol.5, no.2, pp.199–211, 2000.

[5] M. Sitti, "Atomic force microscope probe based controlled pushing for nanotribological characterization, " *IEEE-ASME T. Mech.*, vol.9, no.2, pp.343–349, 2004.

[6] B. Mokaberi and A.A.G. Requicha, "Compensation of Scanner Creep and Hysteresis for AFM Nanomanipulation," *IEEE T. Autom. Sci. Eng.*, vol. 5,no.2, pp. 197-206, 2008.

[7] F. Krohs, C. Onal, M. Sitti, and S. Fatikow, "Towards Automated Nanoassembly With the Atomic Force Microscope: A Versatile Drift Compensation Procedure," *J. Dyn. Syst-T. ASME*, vol. 131, no.131, pp. 636-650, 2009.

[8] Y. Wu, Q. Z. Zou, "Iterative Control Approach to Compensate for Both the Hysteresis and the Dynamics Effects of Piezo Actuators," *IEEE T. Contr. Syst. T.*, vol. 15, no.5, pp. 936-944, 2007.

[9] U. X. Tan, W. T. Latt, C. Y. Shee, and W.T. Ang, "Feedforward Controller of Ill-Conditioned Hysteresis Using Singularity-Free Prandtl-Ishlinskii Model," *IEEE-ASME T. Mech.*, vol. 14, no.5, pp. 598-605, 2009.

[10] J. T. Woodward and D. K. Schwartz, "Removing drift from scanning probe microscope images of periodic samples," *J. Vac. Sci. Technol. B.*, vol. 16, no.16, pp. 51-53, 1998.

[11] B. Mokaberi and A. A. G. Requicha, "Drift compensation for automatic nanomanipulation with scanning probe microscopes," *IEEE T. Autom. Sci. Eng.*, vol. 3, no.3, pp. 199-207, 2006.

[12] Q. Yang, S. Jagannathan,E. W. Bohannan, "Automatic Drift Compensation Using Phase Correlation Method for Nanomanipulation," *IEEE T. Nanotechnol.*, vol. 7, no.2, pp. 209-216, 2008.

[13] H. Xie, and S. Régnier, "High-Efficiency automated nanomanipulation with parallel imaging/manipulation force microscopy, "IEEE T. Nanotechnol., vol.11, no.1, pp.21–33, 2012.

[14] J. J. Leonard and H. F. Durrant-Whyte, "Mobile robot localization by tracking geometric beacons," *IEEE T Robot. Autom.*, vol. 7, no.3, pp. 376-382, 2002.

[15] S. Thrun, W. Burgard, and D. Fox, *Probabilistic Robotics*. London, England: The MIT Press, Cambridge, Massachusetts, 2005.

[16] H. P. Chen, N. Xi, and G. Y. Li, "CAD-guided automated nanoassembly using atomic force microscopy-based nonrobotics," *IEEE T. Autom. Sci. Eng.*, vol. 3, no.3, pp. 208-217, 2006.

[17] C. D. Onal, O. Ozcan, and M. Sitti, "Automated 2-D Nanoparticle Manipulation Using Atomic Force Microscopy," *IEEE T. Nanotechnol.*, vol. 10, no.3, pp. 472-481, 2011.

[18] G. Y. Li, N. Xi, H. P. Chen, C. Pomeroy, and M. Prokos, ""Videolized" atomic force microscopy for interactive nanomanipulation and nanoassembly," *IEEE T. Nanotechnol.*, vol. 4, no.5, pp. 605-615, 2005.

[19] T. Tuma, W. Haeberle, H. Rothuizen, J. Lygeros, A. Pantazi and A. Sebastian, "Dual-Stage Nanopositioning for High-Speed Scanning Probe Microscopy," *IEEE-ASME T. Mech.*, vol. 19, no.3, pp. 1035-1045, 2014.

[20] W. Vogl, M. Bernice Kai-Lam, and M. Sitti, "Augmented reality user interface for an atomic force microscope-based nanorobotic system," *IEEE T. Nanotechnol.*, vol. 5, no.4, pp. 397-406, 2006.

[21] L. Q. Liu, Y. L. Luo, N. Xi, Y. C. Wang, J. B. Zhang and G. Y. Li, "Sensor Referenced Real-Time Videolization of Atomic Force Microscopy for Nanomanipulations," *IEEE-ASME T. Mech.*, vol. 13, no.1, pp. 76-85, 2008.

[22] H. Xie, C. Onal, S. Régnier, and M. Sitti, "Nanomechanics of AFM Based Nanomanipulation," in *Atomic Force Microscopy Based Nanorobotics*. vol. 71, ed: Springer Berlin Heidelberg, 2012, pp. 87-143.

[23] K. Kuhnen and H. Janocha, "Inverse feedforward controller for complex hysteretic nonlinearities in smart-material systems," *Contr. Intell. Syst.*, vol. 29, no.3, pp. 74 ~ 83, 2001.

[24] S. Yuan, L.Q. Liu, Z.D. Wang, N. Xi, Y.C. Wang, Z.L. Dong, *et al.*, "Feature referenced tip localization enhanced by probability motion model for AFM based nanomanipulations," in *Conf. IEEE ROBIO*, 2011, pp. 1421-1426.

[25] Z. Y. Wang, L. Q. Liu, J. Hou, Z. D. Wang, S. Yuan, and Z. L. Dong, "Virtual nano-hand: A stable pushing strategy in AFM based sensorless nanomanipulation," in *Conf. IEEE ROBIO*, 2011, pp. 1409-1414.

[26] C. Jongmoo and G. Medioni, "StaRSaC: Stable random sample consensus for parameter estimation," in *Conf. IEEE CVPR*, pp. 675-682, 2009.

[27] J. Hou, L. Q. Liu, Z. Y. Wang, Z. D. Wang, N. Xi, Y. C. Wang, *et al.*, "AFM-Based Robotic Nano-Hand for Stable Manipulation at Nanoscale," *IEEE T. Autom. Sci. Eng.*, vol. 10, no.2, pp. 285-295, 2013.

[28] Z. Y. Wang, L. Q. Liu, Y. C. Wang, Z. D. Wang, N. Xi, J. Hou, *et al.*, "Stable Nanomanipulation Using Atomic Force Microscopy: A virtual nanohand for a robotic nanomanipulation system," *IEEE Nanotechnol. Mag.*, vol. 7, no.4, pp. 6-11, 2013.

[29] M. Loganathan, A. Al-Ogaidi, and D. A. Bristow, "Design and Control of a Dual-Probe Atomic Force Microscope," *IEEE-ASME T. Mech.*, vol. 23, no. 1, pp. 424-433, 2018.

[30] H. Xie, D. Hussain, F. Yang, L. N. Sun, "Development of Three-Dimensional Atomic Force Microscope for Sidewall Structures Imaging With Controllable Scanning Density," *IEEE-ASME T. Mech.*, vol.21, no.1, pp.316-328, 2016.

Shuai Yuan (M'14) received the B.S. and M.S. degrees from Shenyang Jianzhu University, Shenyang, China, in 2000 and 2003, respectively, and the Ph.D. degree in pattern recognition and intelligent system from the Graduate School of the Chinese Academy of Sciences, Beijing, China, in 2012.

He is currently a Post-Doctoral Researcher with the Shenyang Institute of Automation, Chinese Academy of Sciences, Shenyang. He is also an Associate Professor with the Shenyang Jianzhu University. His research interests include nanorobotics, intelligent control, and image processing.

Zhidong Wang (S'18) received the B.S. degree from the Beijing University of Aeronautics and Astronautics, Beijing, China, in 1987, and the M.Sc. and Ph.D. degrees in engineering from the Graduate School of Engineering, Tohoku University, Sendai, Japan, in 1992 and 1995, respectively.

He is currently a Professor with the Department of Advance Robotics, Chiba Institute of Technology, Chiba, Japan. His current research interests include human–robot interaction and cooperation systems, distributed autonomous robot systems, micro/nano robotics, and application of intelligent robot technologies for the disabled.

Ning Xi (F'07) received the D.Sc. degree in systems science and mathematics from Washington University in St. Louis, St. Louis, MO, USA, in 1993, and the B.S. degree in electrical engineering from the Beijing University of Aeronautics and Astronautics, Beijing, China.

Currently, he is the Chair Professor of Robotics and Automation in the Department of Industrial and Manufacturing System, and the Director of Emerging Technologies Institute of the University of Hong Kong. Before joining the University of Hong Kong, he was the University Distinguished Professor, John D. Ryder Professor of Electrical and Computer Engineering and Director of Robotics and Automation Laboratory at Michigan State University in U.S. He also served as the founding head of the Department of Mechanical and Biomedical Engineering at City University of Hong Kong (2011-2013). His research interests include robotics, manufacturing automation, micro/nano manufacturing, nano sensors and devices, and intelligent control and systems.Prof. Xi served as the President of the IEEE Nanotechnology Council (2010-2011). He has been elected as the President of IEEE Robotics and Automation Society (2018-2019).

Yuechao Wang (M'12) received the M.S. degree in pattern recognition and intelligent control from the Shenyang Institute of Automation, Chinese Academy of Sciences, Shenyang, China, in 1987, and the Ph.D. degree in mechatronic engineering from the Harbin Institute of Technology, Harbin, China, in 1999.

Since 1987, he has been with the Shenyang Institute of Automation, Chinese Academy of Sciences, where he is currently a Professor. His current research interests include robot control, multirobot systems, and micro-nano manipulation.

Lianqing Liu (M'09) received the B.S. degree in industry automation from Zhengzhou University, Zhengzhou, China, in 2002, and the Ph.D. degree from the Shenyang Institute of Automation, Chinese Academy of Sciences, Shenyang, China, in 2009.

He is currently a Professor with the Shenyang Institute of Automation, Chinese Academy of Sciences. His current research interests include nanorobotics, intelligent control, and biosensors. Dr. Liu was awarded the Early Government/Industrial Career Award by the IEEE Robotics and Automation Society in 2011, the Lu Jiaxi Young Scientist Award of the Chinese Academy of Sciences in 2011, and the President Award of the Chinese Academy of Sciences in 2009.